Three-dimensional Dendritic Pt Nanostructures: Sonoelectrochemical Synthesis and Electrochemical Applications

ARTICLE *in* THE JOURNAL OF PHYSICAL CHEMISTRY C · SEPTEMBER 2008

Impact Factor: 4.77 · DOI: 10.1021/jp8060043

6 AUTHORS, INCLUDING:

Qingming Shen
Nanjing University of Posts and Telecomm…
28 PUBLICATIONS **625** CITATIONS
SEE PROFILE

Qianhao Min
Nanjing University
15 PUBLICATIONS **326** CITATIONS
SEE PROFILE

Three-dimensional Dendritic Pt Nanostructures: Sonoelectrochemical Synthesis and Electrochemical Applications

Qingming Shen, Liping Jiang, Hui Zhang, Qianhao Min, Wenhua Hou,* and Jun-Jie Zhu*

School of Chemistry and Chemical Engineering, Key Laboratory of Analytical Chemistry for Life Science (MOE), Key Laboratory of Mesoscopic Chemistry (MOE), Nanjing University, Nanjing, 210093, People's Republic of China

Received: July 8, 2008; Revised Manuscript Received: August 13, 2008

A new and convenient sonoelectrochemical method was used to synthesize uniform three-dimensional (3D) dendritic Pt nanostructures (DPNs) at room temperature. The size and morphology of the final product could be controlled via simply adjusting the experiment parameters. The morphology and structure of the DPNs were characterized by transmission electron microscopy, high resolution transmission electron microscopy, field emission scanning electron microscopy, energy-dispersive X-ray, and X-ray diffraction. The formation process of the DPNs was carefully studied, and a spontaneous assembly mechanism was proposed based on the experimental results. Additionally, the electrocatalytic activity of the DPNs was evaluated using methanol and glucose as model molecules. The DPNs showed improved electrocatalytic activity toward methanol oxidation with respect to the monodisperse Pt nanoparticles; this improvement is due to the porosity structure and the greatly enhanced effective surface area. In addition, a sensitive enzyme-free biosensor can be easily developed for the detection of glucose in pH 7.4 phosphate buffer solution. The present method provides a new and simple strategy toward the fabrication of 3D DPNs with extensive applications.

1. Introduction

As one of the most extensively studied metal nanomaterials, platinum has attracted considerable interests because of its importance in many technical applications[1] such as in sensors,[2] biosensors,[3] and other fields.[4] Recently, it serves as a catalyst in direct methanol fuel cells,[5] and photocatalytic water splitting systems have received wide attention.[6]

However, the high cost and limited supply of platinum prevent it from being an efficient commercial catalyst. Because the catalytic efficiency depends on both the size and the shape of platinum, people can increase their catalytic efficiency and reduce the dosage by the fabrication of Pt nanostructures.[7] In past decades, many efforts have been devoted to the preparation of novel nanostructured platinum with specific structural features, such as Pt polyhedral,[8] nanowires,[9] nanotubes,[10] multipods,[11] porous or 3D dendritic structures,[5e,12] and flat dendritic nanosheets.[12a,13] Among them, the porous or 3D dendritic Pt nanostructures (DPNs) have recently attracted intensive research interests because the nanostructures have higher surface area and supply enough absorption sites for all involved molecules in a narrow space. On the other hand, such materials with porosity in three dimensions could allow unlimited transport of the molecules of the medium.[5e,7e,14] As a result, the catalytic activity can be maximized while the usage of Pt is limited.

Up to now, there are two major techniques that have been developed to synthesize the platinum nanostructures. One is to use organic molecules or polymers as capping agents or morphology-directing reagents combined with differing reduction conditions.[5e,12c,d] Although this route can control the morphology of the obtained Pt nanostructures, it usually needs high temperature, expensive regents, and complicated processes. Another approach is a template-based method.[12a] However, this method is restricted by a number of limiting factors that include the preparation and removal of the templates or the limited range of morphological variation. Therefore, it is urgent to develop a new and simple method for the preparation of porous Pt or DPNs to meet the critical needs of a reproducible and controllable synthetic route for technological applications.

Compared with the conventional method, the sonoelectrochemical method, which combines ultrasound and electrochemistry, has been proven to be a fast, simple, and effective route for shape-controlled synthesis of nanostructured materials.[15] This method is accomplished by applying an electric current pulse to nucleate and perform the electrodeposit, followed by a burst of ultrasonic energy that removes the products from the sonic probe cathode.[15] A prominent feature of this method is that the collapsing bubbles produced in liquid solution during sonication can instantaneously generate local spots of high temperature (5000 K), pressure (50 MPa), and cooling rates (10^9 K·s^{-1})[15,16] During the sonic process, the surface state of the nanoparticles falling from the cathode might change under this remarkable condition, and the morphology of the obtained nanoparticles will transform until the surface state becomes stable. Furthermore, the shape and size of these nanomaterials could be controlled by simple adjusting various parameters such as current density, the time of deposition and sonication, temperature, and sonic power.[15] To our knowledge, although several metal nanostructures have been prepared by means of sonoelectrochemical method,[15a−d] platinum nanomaterials have never been made previously by this technique or other similar approach.

Herein, we describe a one-step, nontemplated sonoelectrochemical method for the synthesis of DPNs at room temperature. The morphology and size of these nanostructures can be controlled by varying the experimental conditions. On the basis of the formation process of the DPNs, a spontaneous assembly

* To whom correspondence should be addressed. E-mail: jjzhu@nju.edu.cn (J.-J.Z), whou@nju.edu.cn (W.H.); phone/fax: +86 25 8359 4976.

10.1021/jp8060043 CCC: $40.75
Published on Web 09/25/2008

mechanism was proposed. In addition, due to the porosity in three dimensions, the as-prepared DPNs exhibited extraordinary electrochemical catalytic behavior to the oxidation of methanol and glucose. A sensitive enzyme-free biosensor has been developed for the detection of glucose in pH 7.4 phosphate buffer solution (PBS). The sonoelectrochemical method provides a simple and environmentally friendly strategy for the fabrication of DPNs, which can be desirable for applications in catalysis and biosensors.

2. Experimental Section

2.1. Materials. Hexachloroplatinum(IV) acid hydrate ($H_2PtCl_6 \cdot 6H_2O$), potassium nitrate (KNO_3), and β-D-glucose were purchased from Chinese Shanghai Reagent Co. Polyvinylpyrrolidone (PVP, K30, Mw 40000) and sodium *n*-dodecyl sulfate (SDS) were purchased from Sinopharm Chemical Reagent Co., Ltd. Poly(ethylene glycol)$_{20}$-poly(propylene glycol)$_{20}$-poly(ethylene glycol)$_{20}$ (P123, MW = 5800) and poly diallyl dimethyl ammonium chloride (PDDA, 20 wt % in H_2O) were purchased from Sigma-Adrich. Sulfuric acid (H_2SO_4, 99.99%) and methanol (CH_3OH, anhydrous) were of analytical grade and were used without further purification. Phosphate buffer solution (PBS, 25 mM, pH = 7.4) was prepared by mixing the solutions of K_2HPO_4 and NaH_2PO_4. Different pH values were adjusted with H_3PO_4 or NaOH. All solutions were prepared with Millipore water.

2.2. Sonoelectrochemical Setup. The sonoelectrochemical device employed in our experiments has been described elsewhere.[15] In brief, a titanium horn (ultrasonic liquid processor VC-750, 20 kHz, Sonics and Materials) acts both as the cathode and the ultrasound emitter. The electroactive part of the sonoelectrode is the planar circular surface of an area of 1.23 cm^2 at the bottom of the horn. The immersed cylindrical part is covered by an isolating plastic jacket. This sonoelectrode produces a sonic pulse that is triggered immediately following a current pulse. A CHI6301B electrochemical workstation (CH Instruments Co., USA) is operated in the pulse current regime (without using a reference electrode). A platinum sheet (1.0 × 1.0 cm) is used as a counter electrode. The pulse width of the current was 1.0 s. The resting time of the current pulse was 0.5 s, and the duration of the ultrasonic pulse was 0.3 s.

2.3. Sonoelectrochemical Synthesis of DPNs. First, 3 mL of H_2PtCl_6 (19.3 mmol·L^{-1}) solution and 1 mL of KNO_3 (1 mol·L^{-1}) solution were added into 60 mL of PVP (5 g·L^{-1}) solution while stirring. Then, the solutions were deaerated with nitrogen for at least 15 min before the preparation. The DPNs were produced with a current density of 10 mA·cm^{-2}, ultrasound intensity of approximately 25% of the rated power (about 20 w), and a reaction time of 1.5 h. After the reaction, the resulting brown−black solution was purified by centrifugation, and the precipitate was sequentially washed several times with Millipore water and then dried in air. These DPNs were sufficiently stable in water, even after storage for several months. Various reactions were carried out with different concentrations of reaction reagent and current densities.

2.4. Characterization. The transmission electron microscopy (TEM) images were recorded on a FEI Tecnai-12 microscope with an accelerating voltage of 120 kV. High-resolution TEM (HRTEM) images were taken using a JEOL 2010 microscope at an accelerating voltage of 200 kV. Samples for TEM and HRTEM were prepared by placing two drops of the dispersed nanoparticles solution on a carbon film coated copper grid (400 mesh), and then drying under air. Field emission scanning electron microscopy (FESEM) images were obtained using a LEO 1530VP field emission electron microscope operating at an accelerating voltage of 8 kV. Samples for FESEM were prepared by placing two drops of the dispersed solution on an indium tin oxide (ITO) conductive glass and then drying under air. Wide-angle powder X-ray diffraction (XRD) patterns were obtained with a Philips X'pert Pro X-ray diffractometer (Cu Kα radiation, $\lambda = 0.15418$ nm). The dynamic light scattering (DLS) was analyzed on a BI-200SM system (Brookhaven Instruments Co.) to study the mean particle size and particles size distribution.

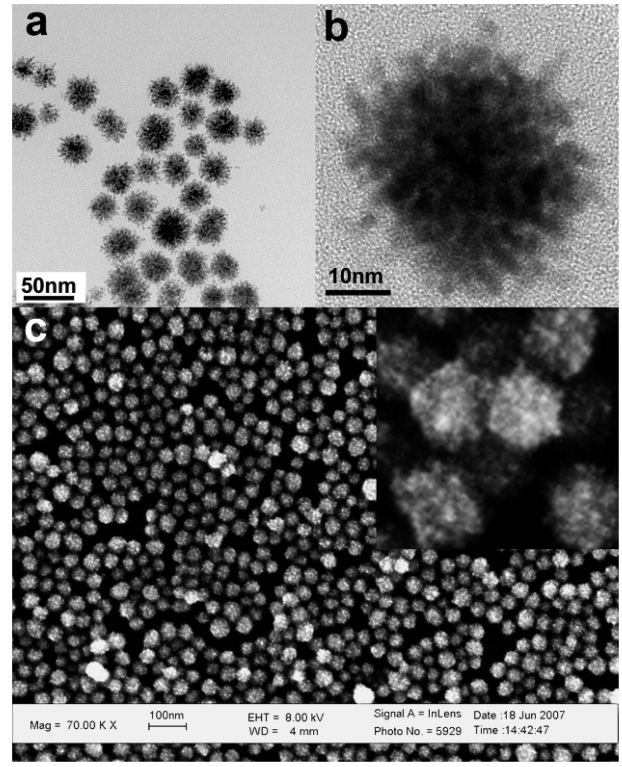

Figure 1. TEM image in (a) low-magnification, (b) high-magnification, and (c) SEM image of DPNs; inset in (c) is the FESEM at high-magnification.

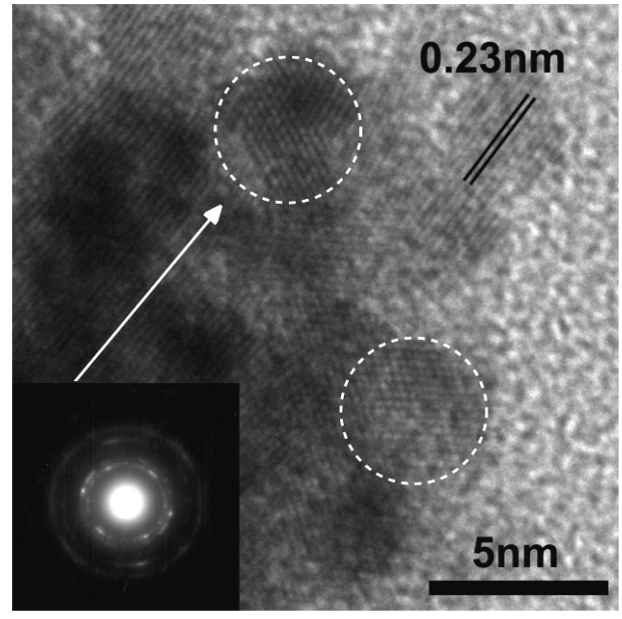

Figure 2. The HRTEM image of a part of the DPNs (lattice spacing discussed in text is indicated, the DPNs is near single crystal, except the circled areas indicating the attached Pt grains). Inset shows the SAED of DPNs.

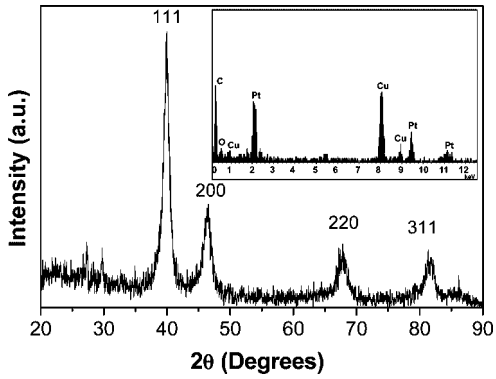

Figure 3. XRD pattern of DPNs. Inset is the EDX spectrum of DPNs.

2.5. Electrocatalytic Study. All electrochemical catalytic activities of Pt nanostructures were characterized using a three-electrode system on an Autolab PGSTAT-30 potentiostat/galvanostat (Eco Chemie BV, The Netherlands). A platinum wire was used as the counter electrode, and a saturated calomel electrode (SCE) was the reference. The working electrode was made of glassy carbon (diameter: 3.0 mm) that was polished with Al_2O_3 powders (Aldrich, 0.05 μm) and rinsed with Millipore deionized water prior to the test. A 10 μL solution of Pt dispersed nanoparticles, which was prepared by sonicating 5 mg of Pt nanoparticles in 10 mL of Millipore water (0.5 mg$\cdot$mL^{-1}), was drop-cast onto a glassy carbon electrode.

Methanol Electrooxidation. The real surface area of the as-prepared Pt-modified electrodes was determined by graphical integration of the area under the hydrogen adsorption peak from -0.172 V (vs SCE) to the double-layer region in a 0.5 M H_2SO_4 solution. Cyclic voltammetry (CV) was conducted in the supporting electrolyte for multiple cycles until a stable curve was obtained. The electrolyte was a 0.5 M H_2SO_4 solution containing 0.5 M CH_3OH, and the electrochemical experiments were carried out in nitrogen-saturated solutions at room temperature. The CV was performed at room temperature. The potential was swept between -0.25 and 1.2 V at a rate of 50 mV$\cdot$s^{-1}.

Glucose Detection. The DPNs/GCE was evaluated as a glucose sensor in a phosphate-buffered saline (PBS, pH = 7.4) solution at desired potentials. The CV was performed at room temperature in PBS solution containing 100 mM glucose at 50 mV$\cdot$s^{-1}. Amperometric curves were obtained after adding the desired concentration of glucose with the solution stirred constantly.

3. Results and Discussion

3.1. Characterization of the DPNs. The morphology and structure of the obtained Pt nanostructures were characterized using TEM, FESEM, and XRD. The low-magnification TEM image in Figure 1a clearly indicates that the obtained Pt nanomaterials are all uniform spherical 3D dendritic structures with a diameter of about 30 nm. The dendritic character of the structures is evident in the high-magnification micrograph, which is built up by tens of primary nanoparticles with an average dimension of 2.5 $\pm$ 0.5 nm (Figure 1b). It appears that these small primary nanoparticles are interconnected with one another to form larger secondary 3D dendritic architectures with recognizable boundaries or voids between the component subunits.

To further confirm the 3D dendritic structure is spherical, the samples were loaded onto an ITO glass for FESEM imaging. The FESEM image in Figure 1c clearly shows the DPNs are truly spherical. The low magnification image also confirms the production of large-scale and narrow size distribution. The inset high-magnification image clearly shows that each DPN is built up by tens of primary nanoparticles about 3 nm in size, which is consistent with the TEM results.

A more detailed examination of the DPNs by high-resolution TEM (HRTEM, Figure 2) shows a lower contrast between the crystallites, which reveals that nanopores separate many primary nanoparticles. It has been previously reported that a larger

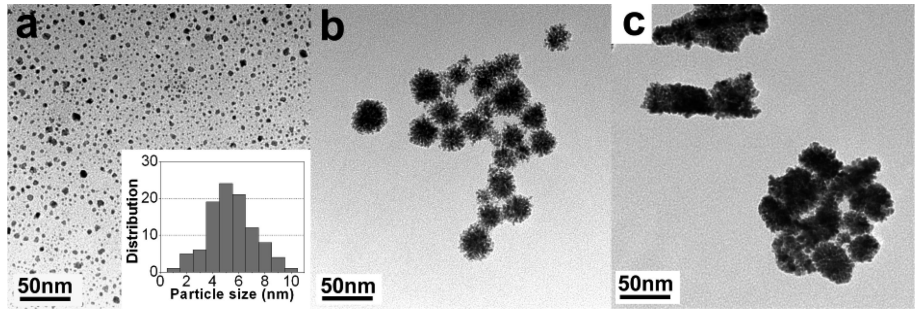

Figure 4. TEM images of the Pt nanostructures at different current densities: (a) 5, (b) 20, and (c) 40 mA$\cdot$cm^{-2}. The inset in panel a is the particle size distribution of the monodisperse Pt nanoparticles.

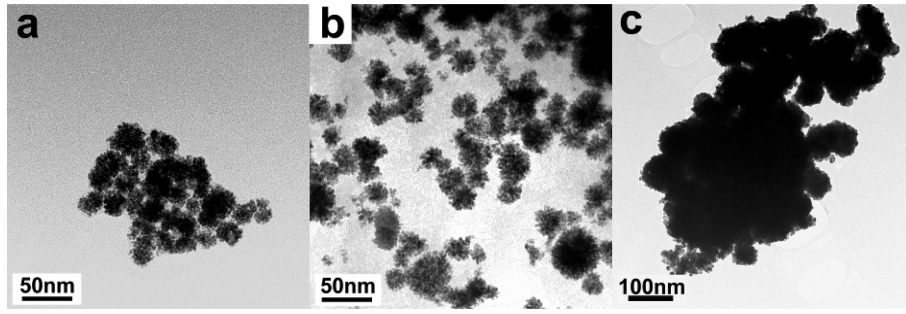

Figure 5. TEM images of the Pt nanostructures synthesized under conditions similar to those used for DPNs, except for the replacement of PVP by other surfactant or polymer: (a) PDDA, (b) P123, and (c) SDS.

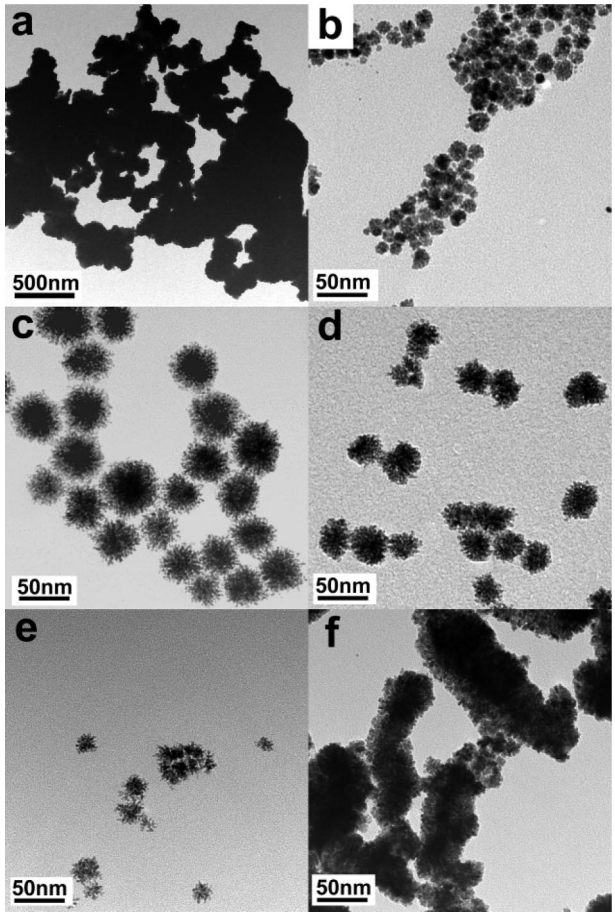

Figure 6. TEM images of Pt nanostructures at different precursor concentration: (a) in the absence of PVP, 1 mM H_2PtCl_6, (b) 2.0 g·L^{-1} PVP, 1 mM H_2PtCl_6, (c) 15.0 g·L^{-1} PVP, 1 mM H_2PtCl_6, (d) 30.0 g·L^{-1} PVP, 1 mM H_2PtCl_6, (e) 5.0 g·L^{-1} PVP, 0.3 mM H_2PtCl_6, and (f) 5.0 g·L^{-1} PVP, 2 mM H_2PtCl_6.

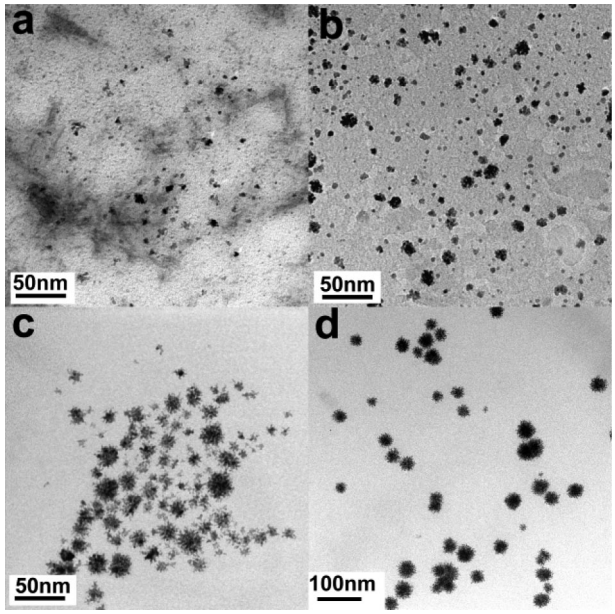

Figure 7. TEM images showing the time development of the DPNs synthesized using sonoelectrochemical method: (a) 10, (b) 30, (c) 60, and (d) 90 min.

crystalline domain can be formed by the small primary nanoparticles via assembly and recrystallization. The clearly marked interplanar *d* spacing is 0.23 nm, which corresponds to that of the {111} lattice planes for face-centered cubic (fcc) Pt.[12a,c] These data suggested that every attached building unit were single crystalline and had different crystallographic orientations in the DPNs. In addition, the Ostwald ripening process of these primary nanoparticles is believed to occur by the coalescence between the individual building units, leading to the formation of a near single crystal, as marked by an arrow, except the circled areas where the Pt grains are just attached. This observation in the HRTEM images is in agreement with the results from the selected area electron diffraction (SAED) pattern of DPNs (inset in Figure 2). In the measured SAED pattern, mainly four kinds of crystalline orientations are observed, which are indexed to be {111}, {200}, {220}, and {311} reflections of (fcc) Pt, but the diffraction spots in all orientations are slightly elongated. The elongated diffraction spots in the SAED pattern suggest the presence of multiple nanodomains with a small misorientation deviating from perfect single crystalline behavior.[12c]

The XRD pattern of platinum nanostructures (Figure 3) reveals that the obtained Pt nanocrystals possess cubic structure with high crystallinity. The four major peaks at about 39.8, 46.4, 67.7, and 81.8° can be assigned to the diffraction from the {111}, {200}, {220}, and {311} planes of the fcc lattice of Pt (JCPDS Card No. 04−0802), respectively. The peak broadening is consistent with the nanoscale structural features of the Pt nanocrystals. By using the Scherrer formula,[17] the mean sizes of the nanocrystals can be calculated from the peak width at half-maximum. The particle size obtained from the width of the {111} reflection is about 2.5 nm. In comparison with the average size of Pt nanocluster obtained from SEM (∼3 nm), it can be easily concluded that DPNs are constructed by Pt primary nanoparticles of average size 2.5 nm.

The chemical composition of the obtained Pt nanostructures was determined using energy-dispersive X-ray (EDX) analysis. In the EDX spectrum (inset in Figure 3), except for the copper and carbon signals from the TEM grid, only peaks of Pt are observed. This result also indicates that the obtained 3D dendritic nanostructures are composed exclusively of platinum.

3.2. Influence of Reaction Parameters on Morphology. To investigate the influence of the reaction parameters on the size and shape of the resulted Pt nanostructures, various reactions were carried out with different current densities, different polymers and surfactants, and different concentrations of reagent.

The current density has a great effect on the morphology of obtained Pt nanostructures. Figure 4 shows the TEM image of Pt nanostructures obtained at different current densities. When the current density was changed from 5 to 40 mA·cm^{-2}, the size and shape of the Pt nanostructures changed remarkably (Figure 4). At a current density of 5 mA·cm^{-2}, monodisperse Pt nanoparticles (MPNs) with a diameter of 6 nm were obtained. When the current density was increased to 20 mA·cm^{-2}, DPNs built up by primary nanoparticles were also obtained (Figure 4b), despite the fact that the DPNs are not uniform, compared with the Figure 1a (10 mA·cm^{-2}). When the current density was further increased to 40 mA·cm^{-2}, the obtained DPNs are agglomerated (Figure 4c). The simple explanation for this is that at low current density (5 mA) the reduction rate of Pt is slower and the number of nuclei is small and the rate of growth is faster than that of nucleation, which lead to the nanoparticles in larger size (5−7 nm), bigger than the primary nanoparticles of DPNs (Figure 1b). On the other hand, the low concentration of these MPNs is not suitable for the assembly of 3D Pt dendritic nanostuctures. As the current density increased (10−20

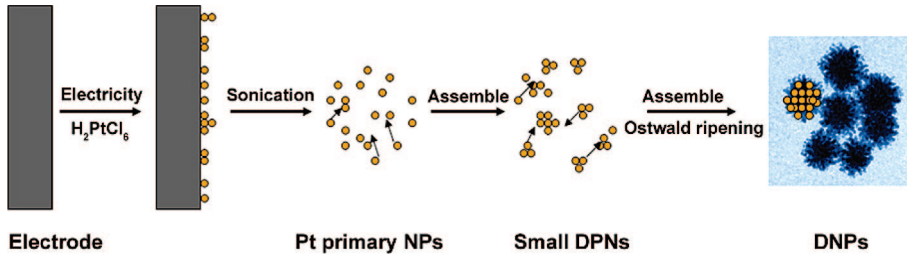

Figure 8. Schematic illustration of the formation of DPNs.

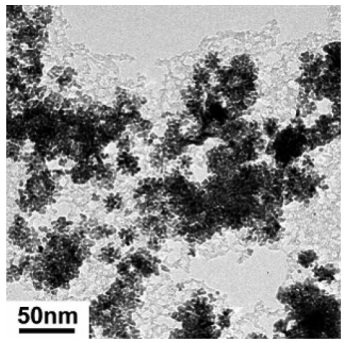

Figure 9. Controlled experiment using ascorbic acid as reducing agent but under the same reaction conditions described above.

$mA \cdot cm^{-2}$), the reduction rate of Pt^{4+} increases and the nucleation rate is faster than that of growth, the enhanced reduction rates leads to the generation of more nuclei and to the formation of smaller primary Pt nanoparticles. As building blocks, these Pt nanoparticles favor the assembly and formation of the DPNs. Nevertheless, when the current density is increased to 40 $mA \cdot cm^{-2}$, the small Pt nanoparticles aggregate further to give random dendritic Pt nanostructures, which is consistent with the previous reports.[15c,e,18]

In addition, we studied the influence of different polymer or surfactant on the morphology of Pt nanostructures. Instead of PVP, the reactions were carried out in the presence of PDDA, P123, and SDS under the same reaction conditions described above. As shown in Figure 5a and Figure 5b, DPNs can also be obtained in PDDA and P123 solutions, respectively, but the obtained DPNs are not uniform and are at a lower yield. In SDS solution, spherical agglomerates of Pt nanoparticles are produced (Figure 5c). These results indicate that by using an appropriate polymer (such as PVP, PDDA, or P123) as stabilizer, the small Pt nanoparticles are all prone to assemble and shape DPNs. This may be due to the Pt−polymer chains interactions that induce the nanoparticle aggregation.[19] Mechanistic studies of the formation of stabilized Pt nanoparticles and their aggregates are consistent with this observation and suggest that the particles are assembled together by attaching to the polymer chains. Because the Pt precursors form stronger bonds with the C═O groups of the PVP,[20] the DPNs synthesized in PVP solution are more uniform than those in other solutions.

To study the effect of precursor concentration on the Pt morphology, the Pt nanostructures obtained at different concentrations of PVP and H_2PtCl_6 were investigated. In the absence of PVP, the agglomerated Pt nanoparticles were obtained (Figure 6a). This indicates that PVP should exist in all these syntheses of DPNs. Otherwise, the Pt nanoparticles would agglomerate into large irregular structures. In a solution of 2 $g \cdot L^{-1}$ PVP, the DPNs with a diameter of 18 nm were synthesized (Figure 6b). With the further increase of PVP concentration, the average diameter of DPNs was increased to 30 nm (5 $g \cdot L^{-1}$ PVP, Figure 1a) and 50 nm (15 $g \cdot L^{-1}$ PVP, Figure 6c). It has also been reported that the metal nanoparticles tend to assemble into spherical nanostructures with moderate concentration of stabilizer (5∼15 $g \cdot L^{-1}$).[9f,19] When the concentration of PVP was increased to 30 $g \cdot L^{-1}$, poorly grown and nonspherical DPNs with a diameter of 40 nm were obtained (Figure 6d). It means that the superfluous PVP (may be 30 $g \cdot L^{-1}$ or more) can restrain the fabrication of the spherical DPNs.

The Pt salt concentration also does have a great effect on the resulting Pt morphology. As the concentration of H_2PtCl_6 decreases to 0.3 mM, the amount of primary nanoparticles decreases, which will lead to the poor growth of DPNs; hence, the size and density of DPNs decreases (Figure 6e). On the contrary, when the concentration of H_2PtCl_6 increases to 2 mM, the amount of primary nanoparticles increases, these primary nanoparticles aggregate further and form irregular and agglomerate Pt nanostructures (Figure 6f).

3.3. Evolution of the Morphology during the Sonoelectrochemical Process. To investigate the growth process of the DPNs, the evolution of the morphology in the sonoelectrochemical synthesis was studied. The TEM images of these samples are shown in Figure 7. When the reaction time was 10 min, individual particles were observed with diameters of about 2.5 nm (Figure 7a). At 30 min of reaction, with the formation of primary nanoparticles, the small 3D dendritic structures formed due to the attachment and assembly of primary nano-

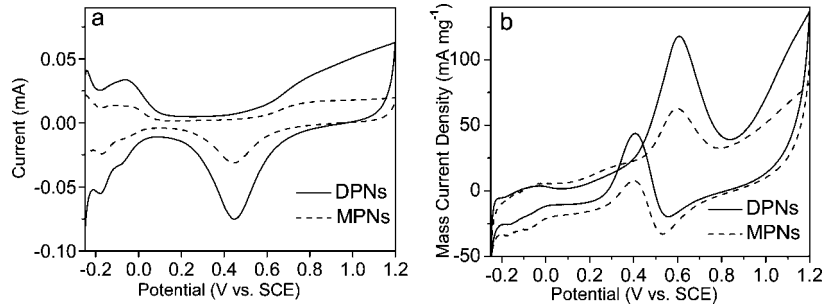

Figure 10. CV plots of DPNs/GCE and MPNs/GCE in a N_2-saturated 0.5 M H_2SO_4 aqueous solution in the absence (a) and presence (b) of 0.5 M methanol measured at a scan rate of 50 mV s^{-1}.

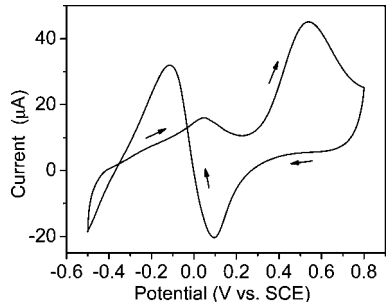

Figure 11. CV of the GPNs/GCE in 0.1 M PBS solution containing 50 mM glucose at 50 $mV \cdot s^{-1}$.

particles (Figure 7b). When the reaction time was prolonged to 60 min, the 3D dendritic structures grew up continuously, and the percentage of the dendritic nanostructures was prevailing (Figure 7c). As the reaction time reached 90 min, the 3D dendritic nanostructures were fully developed and showed a uniform spherical morphology (Figure 7d).

3.4. Mechanism. Recently, similar spherical 3D dendrites were also observed by others in the cases of Rh,[19b] Pd,[21] Ni,[22] Ru,[23] and PtRu.[24] Meanwhile, a spontaneous nanoparticle assembly mechanism was suggested for the formation of the Ni, Ru, Pd, Rh, and PtRu nanostructures, and this mechanism may be extended to explain the formation of the DPNs.

According to the evolution of the morphology shown in Figure 7, we have observed the process that the formed primary nanoparticles spontaneously assemble into the final spherical 3D dendritic nanostructures. Figure 8 shows the schematic for the formation of DPNs. First, platinum ions were reduced by electricity and formed platinum primary nanoparticles on the electrode. Then, the platinum primary nanoparticles were separated in the solution by the ultrasonic. Once the amount of primary nanoparticles reached a certain value, they could spontaneously assemble together and formed small DPNs. With the increase of time and the continuous formation of primary nanoparticles, the small DPNs grew up and eventually led to the formation of DPNs with well-spherical morphology. Moreover, under the ultrasonic condition, the Ostwald ripening process is accelerated, which leads to the small primary nanoparticles in favor of the crystallite reorganization and growth of a stable near-single crystal. The crystal lattice in the HRTEM image (Figure 2) confirms that this structure is assembled by primary nanoparticles.

A controlled experiment was also carried out to verify whether the DPNs could be formed without an electrochemical process. The electroreduction process was replaced by adding ascorbic acid (as a reducing agent), with the other reaction conditions the same as described above. As shown in Figure 9, mainly aggregates of nanoparticles with diameter of 5−8 nm were obtained, and few poorly grown DPNs could be observed. According to these results and previous reports, it can be concluded that the right concentration of precursor, appropriate stabilizer (such as PVP), and the combination of electrochemical and sonochemical processes are essential in the formation of the uniform spherical DPNs.

It can be the conclusion that the previous reports and all above results strongly confirm a mechanism of continuous formation of primary nanoparticles by electroreduction and subsequent spontaneous assembly of these nanoparticles into DPNs under the ultrasonic condition.

3.5. Methanol Electrooxidation. To test the practical applications of the DPNs, methanol was first selected for electrocatalytic experiment. It is well-known that Pt nanoparticles have good catalytic activity for the electrochemical oxidation of methanol.[5] The catalytic property of DPNs and MPNs for the direct oxidation of methanol was studied using CV. The electrochemically active specific surface areas of DPNs/GCEs and MPNs/GCE have been evaluated through the hydrogen adsorption region of cyclic voltammograms measured in 0.5 M H_2SO_4 in absence of methanol (Figure 10a). By integrating the charge required for the adsorption of the hydrogen adatoms,[3d,e,25] the active specific surface area of DPNs/GCEs and MPNs/GCE were calculated to be 37.4 and 16.9 cm^2, respectively. The high electrochemically active specific surface area of DPNs could be attributed to the contained pores within the DPNs.

Figure 10b shows the CV curves of DPNs/GCE and MPNs/GCE in a N_2-saturated 0.5 M H_2SO_4 solution containing 0.5 M methanol. The observed methanol oxidation peaks for both DPNs/GCE and MPNs/GCE were at 0.60 V in the forward sweep and at 0.40 V in the backward sweep. The mass peak current density (at 0.60 V) of the DPNs/GCE and MPNs/GCE were 118 and 63 $mA \cdot mg^{-1}$, respectively. It is clear that the catalysis activity of DPNs is about twice that of the MPNs and is higher than the 51 $mA \cdot mg^{-1}$ measured for commercial carbon supported platinum catalyst (Pt/XC-72R, E-Tek, 60% Pt, diameter of Pt is 6 nm) reported previously in the literature.[5e] This fact demonstrated that DPNs/GCE exhibited higher electrocatalytic activity for the oxidation of methanol, compared with that of MPNs/GCE. The remarkably high oxidation current for the DPNs/GCE is directly related to the surface structure of the DPNs. The dendritic structure that contains pores within the particles might play a crucial role in determining the catalytic performance.

In addition, the ratio of the forward anodic peak current (I_f) to the backward anodic peak current (I_b) I_f/I_b of DPNs/GCE has been estimated to be 2.18, which is higher than the value of MPNs/GCE (1.73) and Pt/XC-72 (1.17).[25,26] As we know,

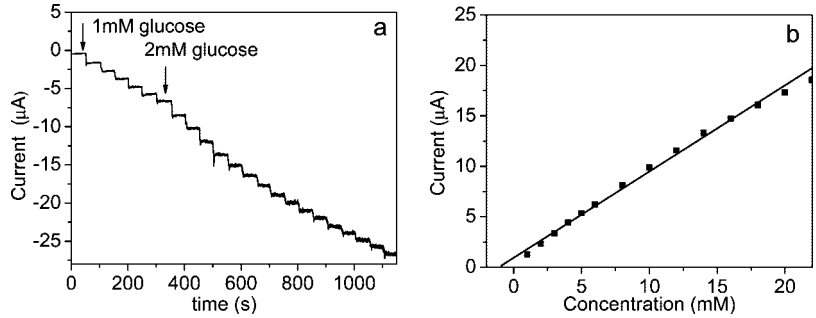

Figure 12. (a) Amperometric response of the DPNs/GCE (at +0.5 V) to successive injections of glucose (glucose was added at the points indicated by arrows to the concentrations mentioned) into PBS. (b) Calibration curve for the electrochemical responses of the DPNs/GCE to glucose in PBS solution.

the I_f/I_b ratio has generally been used to evaluate the tolerance of the catalysts to incompletely oxidized species accumulated on the surface of the electrode.[25,26] The higher I_f/I_b ratio value indicating more methanol oxidized to carbon dioxide and that the concentration of intermediate species on the Pt is relatively lower. Therefore, the higher tolerance of the catalysts to incompletely oxidized species is another important reason for the higher efficiency of DPNs/GCE.

According to the detailed analyses presented above, it is clear that the unique structure of the DPNs results in its superior catalytic properties for the electrochemical oxidation of methanol. The interconnected structure of DPNs not only leads to a high surface area, but also provides enough absorption sites for involved molecules in a limited space.[5e,14] In addition, the good tolerance of the catalysts to the intermediate species also has an advantage in enhancing the catalytic activities.

3.6. Glucose Detection. Further study showed that DPNs/GCE also had an extraordinary electrocatalytic activity toward the oxidation reaction of glucose and could be used as an excellent sensor for the detection of glucose. It is known that Pt nanoparticles show a high electrocatalytic activity for the nonenzymatic detection of glucose.[3] The practical performance of glucose biosensors is usually tested under physiological conditions. Therefore, the electrocatalytic activity of the DPNs/GCE toward glucose was investigated in a PBS solution (pH = 7.4).

The CV of the DPNs/GCE in a PBS solution with 50 mM glucose at a scan rate of 50 $mV \cdot s^{-1}$ is shown in Figure 11. The CV in the positive potential scan process showed two anodic current peaks located at 0.04 and 0.54 V. The first peak should be attributed to the electrosorption of glucose to form adsorbed intermediate, releasing one proton per glucose molecule. With the electrosorption of glucose, the intermediates accumulate and occupy the active sites on the gold electrode surface and as a result the current decreased. With the potential moving to more positive values, Pt-OH starts to form, which can catalyze the oxidation of the poisoning intermediates, releasing free Pt active sites for the direct oxidation of glucose. Therefore, the second current peak at 0.54 V for this direct oxidation appears. The decrease in current after the second current should be due to the formation of Pt oxide, which competes for adsorption sites with glucose and inhibits the direct electrochemical oxidation of glucose as well. In the negative potential scan process, the surface Pt oxide was reduced, and enough surface active sites will be available for the direct oxidation of glucose, leading to an anodic current peak at −0.11 V.[3]

Figure 12a shows the typical steady-state amperometric response of glucose in pH 7.4 PBS, at a detection potential of +0.50 V. The corresponding calibration curve is shown in Figure 12b. The DPNs/GCE respondes to glucose with a good linear dependence in a glucose concentration range from 1.0 to 20 mM. The upper-limit of linear range is 20 mM, which is far beyond the physiological level (3−8 mM), and the detection limit is down to 1.2 μM with a sensitivity of 12.10 $\mu A \cdot cm^{-2} \cdot mM^{-1}$ estimated at a signal-to-noise ratio of 3. The value of sensitivity is larger than the value of 9.6 $\mu A \cdot cm^{-2} \cdot mM^{-1}$ of mesoporous platinum,[3b] which indicates that DPNs have higher sensitivity for glucose detection. The response of DPNs to glucose can reach 95% steady-state value within 2 s. It is also worth noting that DPNs/GCE displays a nice reproducibility with a relative standard deviation of 2.7% by monitoring the current response for six replicate injections of 5.0 mM glucose. These results demonstrate that the present DPNs/GCE could be used as an excellent nonenzymatic sensor for the detection of glucose.

4. Conclusions

In conclusion, we have developed a simple sonoelectrochemical method for the synthesis of DPNs. The size, shape, and uniformity of the Pt nanostructures can be well controlled by the current density and other experiment parameters. The formation of the DPNs is most likely a spontaneous assembly mechanism. The DPNs exhibit good activity for the oxidation of methanol and for the detection of glucose, making them potentially useful in electrocatalytic applications such as in fuel cells or as biosensors. This simple approach can be a useful method for making nanostructures of other noble metals with different morphologies, which can be used in the fields of catalysis and biosensors.

Acknowledgment. We are grateful to the financial support of the European Community Sixth Framework Program through a STREP grant to the SELECTNANO Consortium (Contract No. 516922), the National Natural Science Foundation of China (20635020, 20521503, 20773065), and 973 Program (2007CB-936302).

References and Notes

(1) (a) Scott, D. S.; Hafele, W. *Int. J. Hydrogen Energy* **1990**, *15*, 727. (b) Kordesch, K. V.; Simader, G. R. *Chem. Rev.* **1995**, *95*, 191. (c) Service, R. F. *Science* **1999**, *285*, 682.

(2) (a) Makto, I.; Gaidi, M.; Hazemann, J. L.; Chenevier, B.; Labeau, M. *Sens. Actuators, B* **1999**, *59*, 210. (b) Matsumiya, M.; Shin, W.; Izu, N.; Murayama, N. *Sens. Actuators, B* **2003**, *93*, 309. (c) Bittencourt, C.; Llobet, E.; Ivanov, P.; Correig, X.; Vilanova, X.; Brezmes, J.; Hubalek, J.; Malysz, K.; Pireaux, J. J.; Calderer, J. *Sens. Actuators, B* **2004**, *97*, 67.

(3) (a) Sun, Y. P.; Buck, H.; Mallouk, T. E. *Anal. Chem.* **2001**, *73*, 1599. (b) Park, S.; Chung, T. D.; Kim, H. C. *Anal. Chem.* **2003**, *75*, 3046. (c) Hrapovic, S.; Liu, Y. L.; Male, K. B.; Luong, J. H. T. *Anal. Chem.* **2004**, *76*, 1083. (d) Song, Y. Y.; Zhang, D.; Gao, W.; Xia, X. H. *Chem.—Eur. J.* **2005**, *11*, 2177. (e) Yuan, J. H.; Wang, K.; Xia, X. H. *Adv.Funct. Mater.* **2005**, *15*, 803.

(4) (a) Roach, P. R.; Takano, Y.; Hilleke, R. O.; Vrtis, M. L.; Jin, D.; Sarma, B. K. *Cryogenics* **1986**, *26*, 319. (b) De, S.; Pal, A.; Pal, T. *Langmuir* **2000**, *16*, 6855. (c) Schulz, J.; Roucoux, A.; Patin, H. *Chem. Rev.* **2002**, *102*, 3757. (d) Melosh, N. A.; Boukai, A.; Diana, F.; Cerardot, B.; Badolato, A.; Petroff, P. M.; Heath, J. R. *Science* **2003**, *300*, 112.

(5) (a) Williams, K. R.; Burstein, G. T. *Catal. Today* **1997**, *38*, 401. (b) Pino, L.; Recupero, V.; Beninati, S.; Shukla, A. K.; Hegde, M. S.; Bera, P. *Appl. Catal., A* **2002**, *225*, 63. (c) Rolison, D. R. *Science* **2003**, *299*, 1698. (d) Antolini, E. *Mater. Chem. Phys.* **2003**, *78*, 563. (e) Teng, X. W.; Liang, X. Y.; Maksimuk, S.; Yang, H. *Small* **2006**, *2*, 249.

(6) (a) Cameron, P. J.; Peter, L. M.; Zakeeruddin, S. M.; Gratzel, M. *Coord. Chem. Rev.* **2004**, *248*, 1447. (b) Fang, X. M.; Ma, T. L.; Guan, G. Q.; Akiyama, M.; Abe, E. *J. Photochem. Photobiol.* **2004**, *164*, 179.

(7) (a) Ahmadi, T. S.; Wang, Z. L.; Green, T. C.; Henglein, A.; El-Sayed, M. A. *Science* **1996**, *272*, 1924. (b) Narayanan, R.; El-Sayed, M. A. *Nano Lett.* **2004**, *4*, 1343. (c) Narayanan, R.; El-Sayed, M. A. *J. Am. Chem. Soc.* **2004**, *126*, 7194. (d) Narayanan, R.; El-Sayed, M. A. *Langmuir* **2005**, *21*, 2027. (e) Lee, H.; Habas, S. E.; Kweskin, S.; Butcher, D.; Somorjai, G. A.; Yang, P. D. *Angew. Chem., Int. Ed.* **2006**, *45*, 7824. (f) Xiong, Y. J.; Wiley, B. J.; Xia, Y. N. *Angew. Chem., Int. Ed.* **2007**, *46*, 7157.

(8) (a) Ahmadi, T. S.; Wang, Z. L.; Henglein, A.; El-Sayed, M. A. *Chem. Mater.* **1996**, *8*, 1161. (b) Petroski, J. M.; Wang, A. L.; Green, T. C.; El-Sayed, M. A. *J. Phys. Chem. B* **1998**, *102*, 3316. (c) Teranishi, T.; Kurita, R.; Miyake, M. *J. Inorg. Organomet. Polym.* **2000**, *10*, 145. (d) Miyazaki, A.; Nakano, Y. *Langmuir* **2000**, *16*, 7109. (e) Song, H.; Kim, F.; Connor, S.; Somorjai, G. A.; Yang, P. D. *J. Phys. Chem. B* **2005**, *109*, 188. (f) Ren, J. T.; Tilley, R. D. *J. Am. Chem. Soc.* **2007**, *129*, 3287.

(9) (a) Han, Y.; Kim, J.; Stucky, G. D. *Chem. Mater.* **2000**, *12*, 2068. (b) Shin, H. J.; Ryoo, R.; Liu, Z.; Terasaki, O. *J. Am. Chem. Soc.* **2001**, *123*, 1246. (c) Fu, X. Y.; Wang, Y.; Wu, N. Z.; Gui, L. L.; Tang, Y. Q. *J. Mater. Chem.* **2003**, *13*, 1192. (d) Chen, J. Y.; Herricks, T.; Geissler, M.; Xia, Y. N. *J. Am. Chem. Soc.* **2004**, *126*, 10854. (e) Chen, J. Y.; Herricks, T.; Xia, Y. N. *Angew. Chem., Int. Ed.* **2005**, *44*, 2589. (f) Chen, J. Y.; Xiong, Y. J.; Yin, Y. D.; Xia, Y. N. *Small* **2006**, *2*, 1340. (g) Song, Y. J.; Garcia, R. M.; Dorin, R. M.; Wang, H.; Qiu, Y.; Coker, E. N.; Steen, W. A.; Miller, J. E.; Shelnutt, J. A. *Nano Lett.* **2008**, *5*, 885.

(10) (a) Mayers, B.; Jiang, X.; Sunderland, D.; Cattle, B.; Xia, Y. N. *J. Am. Chem. Soc.* **2003**, *125*, 13364. (b) Sun, Y. G.; Mayers, B.; Xia, Y. N. *Adv. Mater.* **2003**, *15*, 641. (c) Kijima, T.; Yoshimura, T.; Uota, M.; Ikeda, T.; Fujikawa, D.; Mouri, S.; Uoyama, S. *Angew. Chem., Int. Ed.* **2004**, *43*, 228.

(11) (a) Herricks, T.; Chen, J. Y.; Xia, Y. N. *Nano Lett.* **2004**, *4*, 2367. (b) Teng, X. W.; Yang, H. *Nano Lett.* **2005**, *5*, 885. (c) Chen, J. Y.; Herricks, T.; Xia, Y. N. *Angew. Chem., Int. Ed.* **2005**, *44*, 2589.

(12) (a) Song, Y. J.; Yang, Y.; Medforth, C. J.; Pereira, E.; Singh, A. K.; Xu, H. F.; Jiang, Y. B.; Brinker, C. J.; van Swol, F.; Shelnutt, J. A. *J. Am. Chem. Soc.* **2004**, *126*, 635. (b) Ullah, M. H.; Chung, W. S.; Kim, I.; Ha, C. S. *Small* **2006**, *2*, 870. (c) Zhong, X. H.; Feng, Y. Y.; Lieberwirth, I.; Knoll, W. *Chem. Mater.* **2006**, *18*, 2468. (d) Zhang, H. T.; Ding, J.; Chow, G. M. *Langmuir* **2008**, *24*, 375.

(13) Song, Y. J.; Steen, W. A.; Pena, D.; Jiang, Y. B.; Medforth, C. J.; Huo, Q. S.; Pincus, J. L.; Qiu, Y.; Sasaki, D. Y.; Miller, J. E.; Shelnuttt, J. A. *Chem. Mater.* **2006**, *18*, 2335.

(14) (a) Shukla, A. K.; Raman, R. K. *Ann. Rev. Mater. Res.* **2003**, *33*, 155. (b) Rolison, D. R. *Science* **2003**, *299*, 1698.

(15) (a) Reisse, J.; Caulier, T.; Deckerkheer, C.; Fabre, O.; Vandercammen, J.; Delplancke, J. L.; Winand, R. *Ultrason. Sonochem.* **1996**, *3*, S147. (b) Zhu, J. J.; Liu, S. W.; Palchik, O.; Koltypin, Y.; Gedanken, A. *Langmuir* **2000**, *16*, 6396. (c) Haas, I.; Shanmugam, S.; Gedanken, A. *J. Phy. Chem. B* **2006**, *110*, 16947. (d) Haas, I.; Gedanken, A. *Chem. Commun.* **2008**, *15*, 1795. (e) Zhu, J. J.; Aruna, S. T.; Koltypin, Y.; Gedanken, A. *Chem. Mater.* **2000**, *12*, 143. (f) Qiu, X. F.; Burda, C.; Fu, R. L.; Pu, L.; Chen, H. Y.; Zhu, J. J. *J. Am. Chem. Soc.* **2004**, *126*, 16276. (g) Shen, Q. M.; Jiang, L. P.; Miao, J. J.; Hou, W. H.; Zhu, J. J. *Chem. Commun.* **2008**, *14*, 1683.

(16) (a) Mason, T. J.; Walton, J. P.; Lorimer, D. J. *Ultrasonics* **1990**, *28*, 333. (b) Suslick, K. S.; Choe, S. B.; Cichovlas, A. A.; Grinstaff, M. W. *Nature* **1991**, *353*, 414.

(17) Cullity, B. D. *Elements of X-ray Diffraction*, 2nd ed.; Addison-wesley: Reading, MA, 1978; p 102.

(18) (a) Reetz, M. T.; Helbig, W. *J. Am. Chem. Soc.* **1994**, *116*, 7401. (b) Rodrigues-Sanchez, L.; Blanco, M. C.; Lopez-Quintela, M. A. *J. Phys. Chem. B* **2000**, *104*, 9683.

(19) (a) Boal, A. K.; Ilhan, F.; DeRouchey, J. E.; Thurn-Albrecht, T.; Russell, T. P.; Rotello, V. M. *Nature* **2000**, *404*, 746. (b) Shin, H. S.; Yang, H. J.; Kim, S. B.; Lee, M. S. *J. Colloid Interface Sci.* **2004**, *274*, 89. (c) Ewers, T. D.; Sra, A. K.; Norris, B. C.; Cable, R. E.; Cheng, C. H.; Shantz, D. F.; Schaak, R. E. *Chem. Mater.* **2005**, *17*, 514.

(20) (a) Borodko, Y.; Habas, S. E.; Koebel, M.; Yang, P. D.; Frei, H.; Somorjai, G. A. *J. Phys. Chem. B* **2006**, *110*, 23052. (b) Borodko, Y.; Humphrey, S. M.; Tilley, T. D.; Frei, H.; Somorjai, G. A. *J. Phys. Chem. C* **2007**, *111*, 17.

(21) (a) Antonietti, M.; Goltner, C. *Angew. Chem., Int. Ed.* **1997**, *36*, 910. (b) Ramirez, E.; Jansat, S.; Philippot, K.; Lecante, P.; Gomez, M.; Masdeu-Bulto, A. M.; Chaudret, B. *J. Organomet. Chem.* **2004**, *689,* 4601.

(22) Ould-Ely, T.; Amiens, C.; Chaudret, B.; Snoeck, E.; Verelst, M.; Respaud, M.; Broto, J. M. *Chem. Mater.* **1999**, *11*, 526.

(23) (a) Vidoni, O.; Philippot, K.; Amiens, C.; Chaudret, B.; Balmes, O.; Malm, J. O.; Bovin, J. O.; Senocq, F.; Casanove, M. J. *Angew. Chem., Int. Ed.* **1999**, *38*, 3736. (b) Pelzer, K.; Vidoni, O.; Philippot, K.; Chaudret, B.; Colliere, V. *Adv. Func. Mater.* **2003**, *13*, 118.

(24) Teng, X. W.; Maksimuk, S.; Frommer, S.; Yang, H. *Chem. Mater.* **2007**, *19*, 36.

(25) Wen, Z. H.; Wang, Q.; Li, J. H. *Adv. Func. Mater.* **2008**, *18*, 959.

(26) (a) Lin, Y. H.; Cui, X. L.; Yen, C.; Wai, C. M. *J. Phys. Chem. B* **2005**, *109*, 14410. (b) Liu, F.; Lee, J. Y.; Zhou, W. J. *Small* **2006**, *2*, 121.

JP8060043